DEBRIS AERODYNAMIC INTERACTION AND ITS EFFECT ON RE-ENTRY RISK ASSESSMENT

Y. Prevereaud[(1)], J-L. Verant[(2)], J-M. Moschetta[(3)], and F. Sourgen[(4)]

[(1)] *ONERA - The French Aerospace Lab, 31 055 Toulouse, France, Email: Ysolde.Prevereaud@onera.fr*
[(2)] *ONERA - The French Aerospace Lab, 31 055 Toulouse, France, Email: Jean-Luc.Verant@onera.fr*
[(3)] *ISAE - Institut Supérieur de l'Aéronautique et de l'Espace, 31 055 Toulouse, France, Email: jean-marc.moschetta@isae.fr*
[(4)] *ONERA - The French Aerospace Lab, 31 055 Toulouse, France, Email: Frederic.Sourgen@onera.fr*

ABSTRACT

Aerodynamic interactions of objects in a continuum hypersonic and supersonic flow are numerically and analytically investigated for perfect and thermochemical equilibrium gas conditions. An innovative semi-analytical methodology has been developed and associated to the Laurence equations [4] in order to compute the aerodynamics coefficients of a sphere located downstream the shock wave issued from a primary object. The influence of the aerodynamic interactions on the trajectory of a debris cloud during atmospheric re-entry has also been assessed and compared to the trajectory of the same non-interacting objects. Finally, the influence of fragments interactions on heat flux and debris survivability during the re-entry has been investigated.

Key words: Space debris; Interaction; Aerothermodynamics; Atmospheric re-entry; Risk.

1. INTRODUCTION AND CONTEXT

SINCE 1957 and the orbital performance of the soviet satellite Spoutnik-1, the human activity in space has generated a great number of space debris. The increase of fragments produced by in-orbit collisions, combined to the hard atmospheric drag in low Earth orbits and polar orbits, could lead to an increasing number of uncontrolled atmospheric re-entries for the next decades. Indeed, over the last forty years, about 16,000 tons of these objects ranging from ten microns to several meters have done an atmospheric re-entry. Between 10 to 40 percent of that mass are estimated to have reached the ground [1]. Occasionally, debris having a projected area superior or equal to 100 m^2 and weighting more than 10 tons could also perform atmospheric re-entry. That kind of objects can be classified as highly hazardous with regard to the great number of fragments produced during re-entry which are able to survive to the critical aerothermodynamic environment. Therefore, they represent a potential threat to ground safety.

Several space agencies and research institutes have developed tools to predict the atmospheric re-entry of space debris and to assess their total casualty area, impact location as well as the state in which the elements may reach the ground. At the present time, according to public literature, seven major atmospheric re-entry codes have been developed through the world. They can be divided into two categories: object-oriented codes and spacecraft-oriented codes.

Object-oriented codes only analyze individually the satellite elements performing re-entry. In other words, this kind of code assumes that, at a given altitude, usually set between 75 to 85 kilometers, the satellite is broken down into its elementary parts and scattered. Then, these ones are followed independently during re-entry phase (there is no physical model of fragmentation, the break-up altitude is empirical). Therefore, the atmospheric re-entry analysis of a whole satellite is replaced within the individual analysis of its most critical parts. The six object oriented codes known are : DAS (NASA), ORSAT (NASA), ORSAT-J (JAXA), DRAMA/SESAM (ESA), Debrisk (CNES) and DRAPS (China).
The spacecraft-oriented codes, whose SCARAB (ESA-HTG Germany) is currently the unique code known, consist of modeling the complete satellite, as close as possible to the real one. The fragmentation and/or ablation of the spacecraft model depends on the aerothermodynamic environment encountered during the atmospheric re-entry. After the fragmentation has occurred, each element is individually analyzed.

However, the great number of fragments actually generated during re-entry may evolve independently, or, on the contrary, interact one another for a while. In addition, a fragment, moving into the wake generated by the main object, is submitted to very different aerothermodynamic conditions as compared to those located upstream. Therefore, one or more objects located in the wake may have a different trajectory and life time than if they were facing the upstream flow. This complex situation, commonly called *aerodynamic interactions or flying formation pro-*

Proc. '6th European Conference on Space Debris'
Darmstadt, Germany, 22–25 April 2013 (ESA SP-723, August 2013)

cess, is not currently taken into account by existing atmospheric re-entry debris codes [2].

Nevertheless, in the literature several authors have experimentally, numerically and analytically investigated the aerodynamics interactions into a given fragments cloud. In particular, Schultz and Sugita [3] (1994) have studied the evolution (the dispersal and the deceleration) of a debris cloud during atmospheric re-entry. Experimental investigations performed at the NASA-Ames Vertical Gun as well as theoretical considerations have allowed them to identify the objects sizes (the dimensionless shock distance), the lateral velocity as well as the atmospheric density which are required to experiment the so called collimation effect [3]. Authors have pointed out the importance of that kind of fragmentation process for the phenomenon to occur.
In terms of numerical simulations, Passey and Melosh [9] (1980) investigated the reasons for cross-range dispersion of fragments in crater fields. They concluded that several physical phenomena could explain the meteoroid fragment scattering. Besides, they pointed out the combined influence of bow shock interactions, deceleration and spinning of the primary fragment. Artemieva and Shuvalov [7], [10] (1996 and 2001) performed numerical simulations of the flow around interacting fragments for different shapes. They computed drag and lift coefficients acting on bodies placed in the primary shock region as a function of their relative positions. In further simulations [10] the authors investigated the repulsive coefficient as a function of the distance between two fragments placed side by side. They coupled their three dimensional hydrodynamic code with a fragmentation model in order to follow the evolution of a few number of fragments. More recently, using CFD, Barri [8] (2010) computed the aerodynamic coefficients acting on a sphere located at different positions in perfect gas conditions in the supersonic regime. She identified the critical values for fragment sizes and positions for the collimation effect can occur. Finally, the original work of Vashchenkov, Kashovsky and Ivanov [11] (2003) should be mentioned since they have investigated forces acting on cylinders placed into the shock region generated by a primary one in the transitional regime ($Kn \sim 0.02$). In the simulations performed using a DSMC method, a very large distance of wake behind the body ($\sim 25 \times d_1$) has been under consideration. Authors have concluded that smaller fragments ($d_2 \leq 0.001 \times d_1$) cannot experience the non-uniformity of the flow. Furthermore, they have pointed out that the secondary fragments could have an influence on the primary one according to the fragment and the subsonic region size.

In anyway, the space debris re-entry trajectory and the survivability issue require the use of codes having short response time due to a necessary sensitivity approach for generation of thousands of trajectories. Therefore, the coupling of a trajectory code with a CFD code, as performed by Artemieva and Shuvalov [7], [10], would be much too expensive with regard to the CPU cost when applied to the whole trajectory computation. Moreover, even the supercomputers could not follow a great number of fragments if interactions are accounted for. In that case, model reduction strategy must be considered.

Laurence [4] (2007) has developed an analytical method, based on Sedov [5] Blast Wave Analogy (BWA), in order to determine the drag and lift coefficients exerting on an infinite cylinder or a sphere located within the primary shock region. The analytical results have been compared to numerical simulations and measurements. A reasonable agreement has been found for most of locations studied for the secondary fragments. Therefore, a number of problems are intrinsic to Sedov BWA. Yet, the BWA is known to underestimate the shock radius as shown in Fig. 2. Furthermore, because of the high Mach number assumption, Sedov-Laurence's method can be used in high hypersonic regime only. According to the author, the blast wave method is in good agreement with numerical results for high speed flows which Mach number is of the order of 50 and higher, which remains an asymptotic case. However, in the case of debris entering the Earth atmosphere, the maximum re-entry velocity value is around $M_\infty \sim 30$. Furthermore, in Sedov-Laurence approach, the flow is assumed to be a perfect gas, which is absolutely not representative of the reality of flows encountered during the atmospheric re-entry. Finally, the blast wave methodology is not valid anymore neither in the wake region located immediately behind the body (for $x/d_1 < 1.5$, according to Laurence) nor far downstream.

The present work aims at developing a new methodology, called semi-analytical methodology, taking into account the real gas effect at thermochemical equilibrium, which would be valid in the whole front fragment shock region, and which would have a short response time in order to quickly compute the debris trajectories. This new methodology will replace the BWA in the Laurence approach. Therefore, in this paper, the interactions between fragments in the hypersonic and supersonic regimes at perfect and thermochemical equilibrium gas conditions are investigated and discussed. Then the influence of fragments interactions on trajectory and debris life time is studied.

2. METHODOLOGY

2.1. Principles of the semi-analytical method

The present semi-analytical method consists of extrapolating, for an other trajectory point, the aerothermodynamics data issued from a numerical reference field (P_{simu}, T_{simu}, $V_{x,simu}$, $V_{y,simu}$). The reference field might be computed by a two dimensional axisymmetric finite volume method (Fig. 1), for instance.
Knowing the free stream conditions encountered at each flight point (ρ_∞, T_∞, V_∞), the first object size (diameter = d_1), the relative position of the secondary fragment with the primary one (x, r) and the numerical reference field conditions - as first object size, $d_{1,simu}$, free stream conditions ($P_{\infty,simu}$, $T_{\infty,simu}$, $V_{\infty,simu}$),

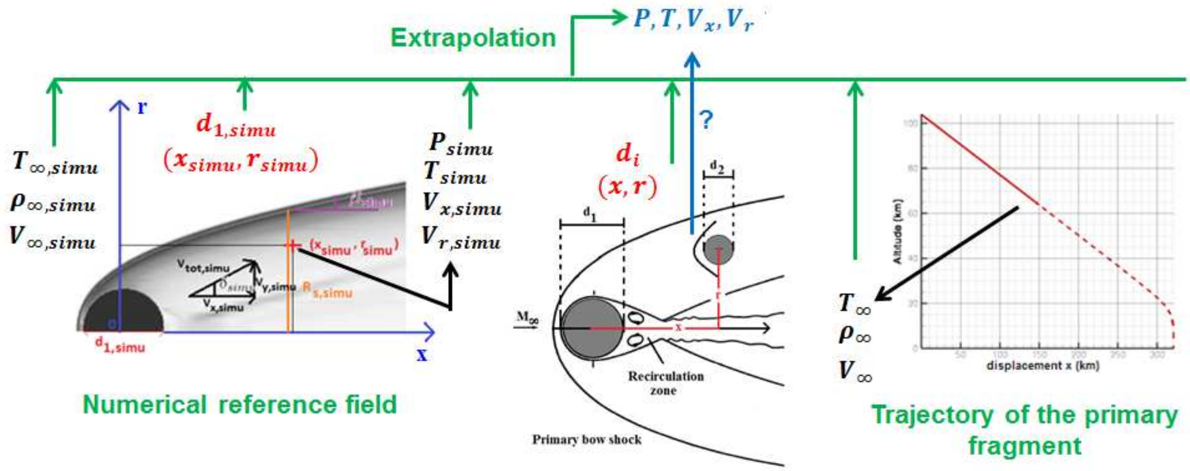

Figure 1. Principle of the semi-analytical method.

aerothermodynamics data for each point (x_{simu}, r_{simu}) of the reference simulation -, then aerothermodynamics flow data (P, T, V_x, V_y) encountered by the secondary object can be assessed.

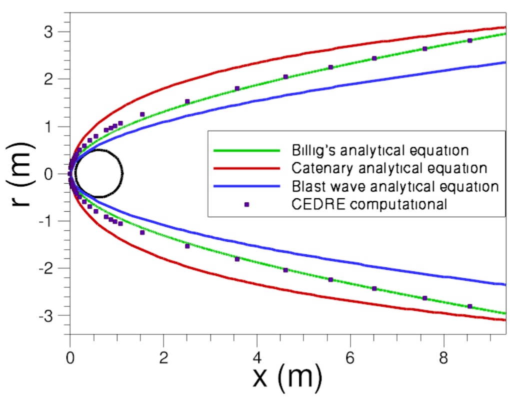

Figure 2. Comparison of analytical shock equations with numerical computations done with the ONERA code CEDRE for a 1 m diameter sphere at M=9.55 for a perfect gas.

Any change in freestream conditions during the atmospheric re-entry would lead to a modification of the flow structure. In particular, the increase or decrease of the upstream Mach number value leads to a compression or an expansion of the shock wave, respectively. Therefore, the first step consists of determining where to select the aerothermodynamics data in the numerical reference flow field in order to develop a formulation for the transformation $(x, r) \rightarrow (x_{simu}, r_{simu})$. In the present paper, it has been chosen to keep x unchanged ($x = x_{simu}$), and to ensure the conservation of flow rate in the wake.

The shock wave plays a key role in the geometrical transformations used in the present method so that its position must be predicted analytically the most accurately as possible. A new relation based on the one obtained by Billig [12] for the vertex radius curvature has been proposed.

$$R_s = a \times tan\left(arcsin\left(\frac{1}{M_\infty}\right)\right)\sqrt{\left(\frac{x_s + a}{a}\right)^2 - 1} \tag{1}$$

With

$$a = b\frac{d_1}{2}exp\left(\left(\frac{c}{M_\infty - 1}\right)^d\right)\frac{1}{tan\left(arcsin\left(\frac{1}{M_\infty}\right)\right)^2} \tag{2}$$

The coefficient b is a function depending only on the Mach number. Eq. 1 is applicable for a perfect gas flow on a large Mach number range from Mach 2 to Mach 9.5. For a gas at thermochemical equilibrium flow, Eq. 1 is valid from Mach 9.5 to Mach 30.

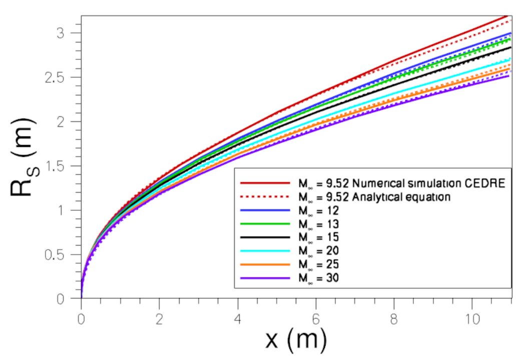

Figure 3. Comparison of the shock radius obtained by the modified shock equation of Billig and numerical results of ONERA code CEDRE. Different values of Mach number for a 1 m diameter sphere are considered and the gas is assumed in thermochemical equilibrium.

2.2. The numerical reference flowfields

The numerical reference flowfields have been performed using the ONERA multi-physics platform CEDRE coupled with the CHARME solver for hypersonic gas flow. A two-dimensional axisymmetric hexa grid of 310 000 nodes has been used. 370 cells are equally distributed in the radial direction around the sphere (Fig. 4). All simulations have been performed on a parallel cluster, and a CFL number equal to 0.5 has been chosen for each of them. The Euler equations have been solved at first spatial order for an ideal gas ($\gamma = 1.4$) and a real gas at thermochemical equilibrium using the flux vector splitting scheme of Van Leer, associated to a Van Leer limiter. The time integration has been set to a one step implicit finite-volume approach.

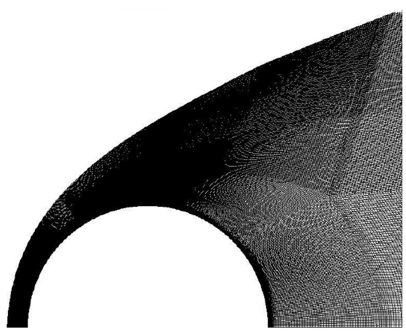

Figure 4. 2D axisymmetric mesh used for the reference field computation assuming gas at thermochemical equilibrium.

2.3. Method validation and limits

The semi-analytical methodology developed in perfect and real gas is now evaluated. The validity range of the semi-analytical method has been established by testing the influence of the infinite speed value and of the altitude (through the variation of the infinite temperature and pressure values) on the aimed extrapolated results compared to numerical simulations of the targeted field. It has been observed that only the Mach number had a significant impact on results. Therefore, in the semi-analytical method, one numerical reference field can be used for extrapolation towards different flight points (different static conditions at a given Mach number). As for the Mach number resolution, a same numerical reference field is used in the range of $M_\infty \pm 0.5$ in the supersonic regime and $M_\infty \pm 2.5$ in the hypersonic regime in order to keep a mean error on pressure lower than 1.5 %. As a matter of fact, a complete atmospheric re-entry ($0 \leq M_\infty \leq 30$ for debris re-entries) can be performed using only nine numerical reference fields. Usually, the nine numerical reference fields used are computed at $H = 0$ km and at different speeds. According to the Mach number grid defined above, any trajectory point can be extrapolated from these reference data.

The ballistic re-entry of a single sphere, representing a hollow Ti_6Al_4V tank of one meter diameter, has been simulated in order to identify flight points of interest Computation has been performed using a 4th-order Runge Kutta scheme and a fixed time step. The hollow sphere enters the atmosphere at 7700 m/s, at an altitude of 78 km and an entry flight path angle of $-1°$. The semi-analytical methodology has been tested on some identified flight points. Two chosen points are presented on Fig. 5 and 6.

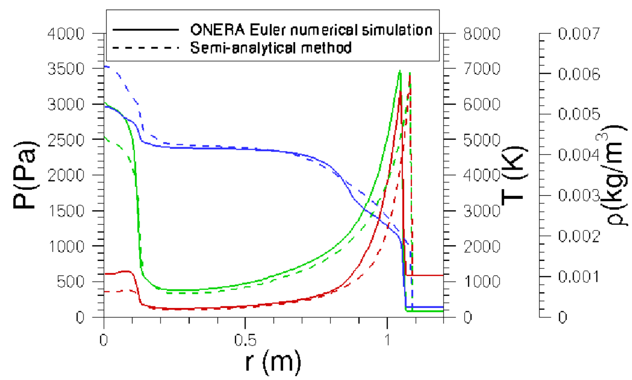

Figure 5. Comparison at fixed $x = 1m$ (from sphere center) of a numerical simulation ($V_\infty = 7400\ m/s$, $H = 50\ km$) with the results extrapolated using the semi-analytical method for a real gas from a numerical reference field computed for $V_\infty = 7634\ m/s$, $P_\infty = 101325\ Pa$ and $T_\infty = 300\ K$. Pressure (green), Temperature (blue), and density (red).

In Fig. 5, the results, issued from the semi-analytical method (using a numerical reference field computed for $V_\infty = 7634\ m/s$, $P_\infty = 101325\ Pa$ and $T_\infty = 300\ K$), are compared with the numerical simulation of the targeted field: the flow around a one meter diameter sphere flying at 7400 m/s and at an altitude of 50 km ($P_\infty = 79.78\ Pa$ and $T_\infty = 270.65\ K$). Pressure, temperature, and density values are compared at station $x = 1\ m$ (center to center), r varying from the axis ($r = 0$) to the shock wave location (R_s). Notice that these results could not be compared with results obtained using the BWA which is based on perfect gas assumption. Fig. 6 displays comparison between numerical and semi-analytical results in conditions of lower velocity ($V_\infty = 2023\ m/s$) and lower altitude ($H = 20\ km$, i.e. $P_\infty = 5530\ Pa$ and $T_\infty = 216\ K$), in perfect gas. In fig. 5 and 6, after the passing across the shock, the aerothermodynamics parameters achieved their freestream values again.

The error produced by the analytical shock equation being smaller, a good agreement between numerical and semi-analytical results can be observed on Fig. 5 and 6, even in the shock region. Indeed, the semi-analytical method is in part based on a geometrical modification of the shock as a function of Mach number variations during the atmospheric re-entry. Therefore, the uncertainty given by the semi-analytical methodology is

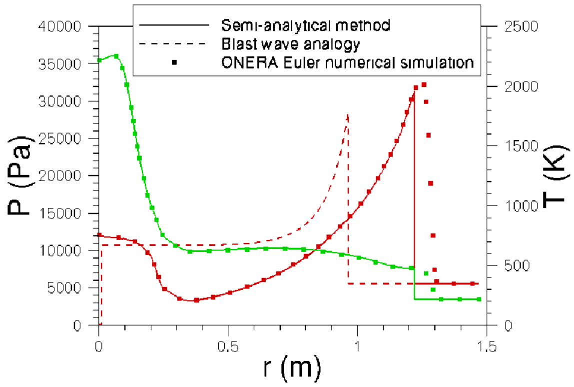

Figure 6. Comparison at fixed $x = 1m$ (from sphere center) of a numerical simulation ($V_\infty = 2023\ m/s$, $H = 20\ km$) with the results extrapolated using the semi-analytical method for a real gas from a numerical reference field computed for $V_\infty = 2430\ m/s$, $P_\infty = 101325\ Pa$ and $T_\infty = 300\ K$. Pressure (red), Temperature (green).

closely linked to the one made in the shock equation.

3. COMPARISON OF ANALYTICAL, SEMI-ANALYTICAL, AND NUMERICAL RESULTS

To determine aerodynamics coefficients for the modified Newtonian profile, the equations of lift (C_L) and drag (C_D) coefficients, proposed by Laurence [4], are used. Moreover, the modifications in aerodynamics coefficients equations proposed by Laurence [4] to take into account the shock-shock interactions, i.e. for $R_s - d_2/2 \leq r \leq R_s + d_2/2$, have been considered here. However, the higher the ratio $\frac{d_1}{d_2}$ is and the less correct the modification proposed by Laurence are (Fig. 7).

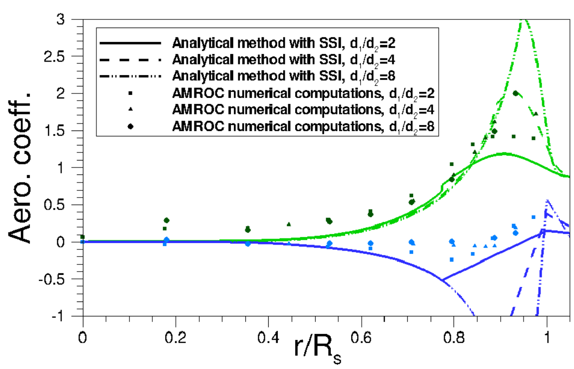

Figure 7. Comparison of lift (blue) and drag (green) coefficients around a secondary sphere in a perfect gas using Sedov-Laurence analytical method and AMR numerical Euler computations (AMROC solver) from Laurence [4], at $M_\infty = 10$, $H = 0\ km$, and $x/d_1 = 1.5$ (center-to-center) for different values of d_1/d_2.

Lift (C_L) and drag (C_D) coefficients, calculated with analytical (Sedov BWA) and present semi-analytical (Prevereaud method) methods on a secondary sphere, are directly compared on Fig. 8, for perfect gas conditions. AMR Euler numerical simulations performed by Laurence [4] (with AMROC solver) for $M_\infty = 10$ and $H = 0\ km$ are used as reference to estimate the level of deviation with analytical/semi-analytical results. Besides, Fig. 9 compares present method with ONERA Navier-Stokes numerical computations (performed thanks to elsA solver) for $M_\infty = 22.4$ and $H = 50\ km$, assuming thermochemical equilibrium gas. In the two cases presented here, the diameter ratio between the primary and secondary fragments, d_1/d_2, are respectively equal to 2 and 4, and various center-to-center lateral and axial displacements are proposed.

The fragment is supposed to be large enough relatively to the shock thickness in order to experience the non-uniformity of the flow. Therefore, a non-zero lift coefficient can be observed on the secondary sphere.

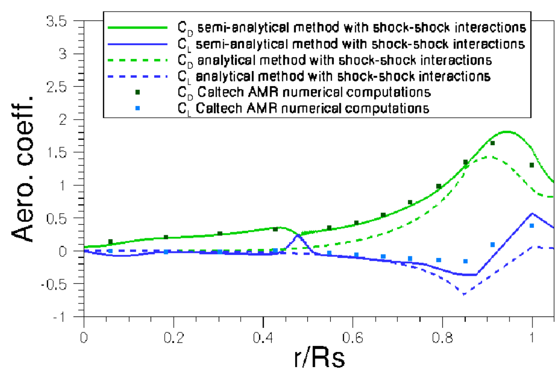

Figure 8. Comparison of lift and drag coefficients around a secondary sphere in a perfect gas using Sedov-Laurence analytical method, present semi-analytical method and AMR numerical Euler computations from Laurence [4], at $M_\infty = 10$, $H = 0\ km$, $d_1/d_2 = 2$ and $x/d_1 = 4$ (center-to-center), Perfect gas condition.

In Fig. 8 a clear improvement is observed with the semi-analytical method. As can be seen in Fig. 9 numerical and semi-analytical results are close. Moreover, in Fig. 8 and Fig. 9, a small peak can be mentioned with computational and semi-analytical results for $r/R_s = 0.48$ and $r = 0.25\ m$ respectively. This is caused by the flow unsteadiness produced by interactions of the secondary sphere with the wake region or the separation shock created by the primary one. Contrarily to the BWA, this effect is present in the semi-analytical method through the numerical reference field, and seems to be well reproduced for other flight points. Nearby the shock, for r/R_s close to 1, lift and drag coefficients significantly increase, due to the impingement of the primary shock wave on the secondary sphere (Fig. 10). As a matter of fact, the distribution of pressure is significantly and obviously affected by shock-shock interactions. Once again, a clear improvement can be observed with the semi-analytical

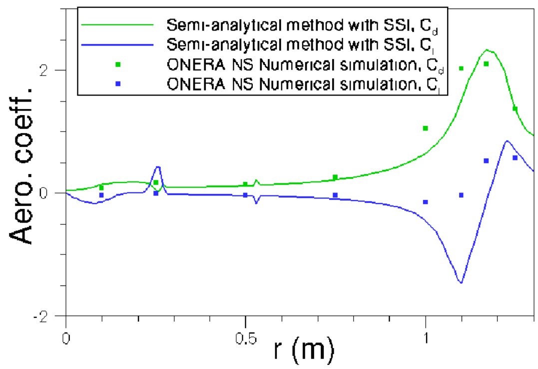

Figure 9. Comparison of lift and drag coefficients around a secondary sphere in gas at equilibrium using present semi-analytical method and elsA numerical Navier-Stokes computations, at $M_\infty = 22.4$, $H = 50$ km, $d_1/d_2 = 4$ and $x/d_1 = 1.5$ (center-to-center), real gas condition.

method in that region (Fig. 8).

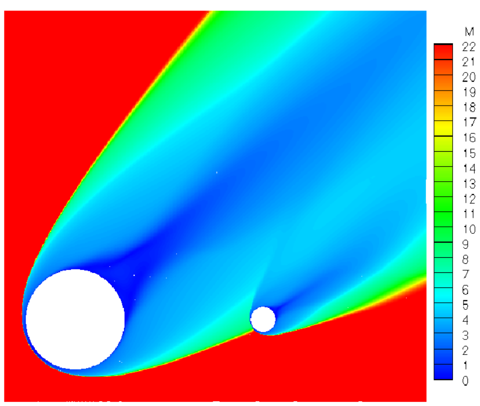

Figure 10. Numerical Navier-Stokes simulation with elsA at $M_\infty = 22.4$, $H = 50$ km, $d_1/d_2 = 4$ and $x/d_1 = 1.5$ (center-to-center)

4. ATMOSPHERIC RE-ENTRY ANALYSIS : INFLUENCE ON DEBRIS TRAJECTORY

In this chapter, the influence of fragments interaction on the trajectory is investigated. The semi-analytical method is then applied to evaluate the influence of fragments interactions on the secondary object trajectory flight.

The primary object is one meter diameter sphere representing a tank of 2 mm wall thickness, made in Ti_6Al_4V. The four-fifth of the tank are supposed to contain frozen hydrazine (N_2H_4) whose density is found equal to 1025 kg/m^3. So, the tank contain 422.4 kg of frozen N_2H_4. The objective was to keep the same conditions than the ones proposed in the study of Kelley and Rochelle [14] on the atmospheric re-entry of an hydrazine tank. Indeed, in their paper, the authors concluded that the tank considered should survived to atmospheric re-entry. In order to study the fragment interactions, the survivability of the primary fragment must be ensured.
The secondary fragment is supposed to embody a hollow Ti_6Al_4V tank of 0.5 meter diameter and 2 mm wall thickness.

The sphere trajectories are performed thanks to the integration of 3-Dof equations of motion describing changes due to the applied forces. Integration is performed, as long as the two bodies have not reached the ground, thanks to a 4^{th}-order Runge-Kutta scheme with a fixed time step. The initial entry velocity of the main fragment is assumed to be in the x-z plane, where the z axis is normal to the Earth surface. The Earth is supposed to be spherical and without rotation. The flow around the bodies behaves as real or perfect gas according to the flight conditions. The two bodies are supposed not to rotate and have no mass loss during the atmospheric re-entry. The atmospheric constant values are taken from tables of the US-76 model with linear interpolation between values.

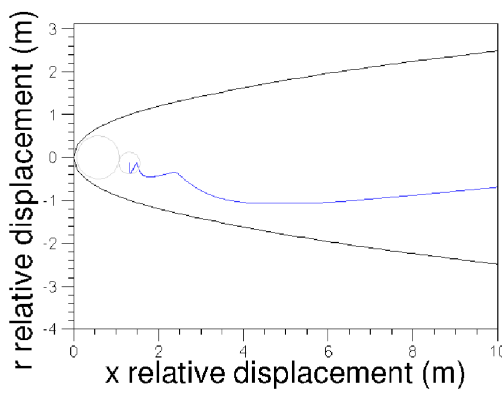

Figure 11. Relative motion of the secondary fragment versus the primary one during the atmospheric reentry

Fig. 11 shows the relative motion of the secondary fragment compared to the primary one. As considered here, the secondary sphere stays in interaction 1.7% of the total re-entry time with the primary one. The consequence on ground dispersion is about 20 km, when fragment interactions are considered or not (Fig. 12).

5. ATMOSPHERIC RE-ENTRY ANALYSIS : INFLUENCE ON DEBRIS SURVIVABILITY

In this chapter, the influence of fragments interaction on the debris survivability is investigated.

$$\Phi_{stored} = \Phi_{conv} + \Phi_{rad,g} - \Phi_{rad,w} + \Phi_{cond} \qquad (3)$$

The heat flux balance is computed only at the stagnation point of the spheres.

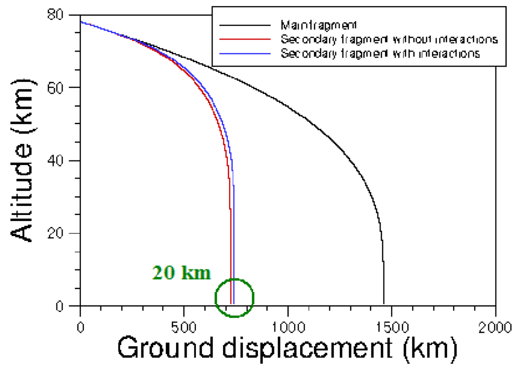

Figure 12. Atmospheric re-entry of the main fragment (black line) and the secondary fragment when fragment interactions are considered (blue line) or not (red line). The fragmentation occurs at 78 km and 7700 m/s.

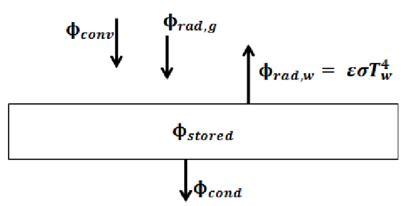

Figure 13. Schematic of the heat flux balance at the stagnation point

The convective heat flux is given by the Verant-Sagnier's formulation [15] :

$$\Phi_{conv} = f(P_{stag}, R_n, \Delta H) \tag{4}$$

Where P_{stag} is the stagnation pressure (Pa), R_n is the nose radius (m), and the enthalpy difference must be $\Delta H > 0\,(J)$,.

The radiative heat flux of the gas is given by the Martin's formulation [16]:

$$\Phi_{rad,g} = C.R_n.\left(\frac{\rho_0}{1.225}\right)^{1.6}.\left(\frac{V_0}{10^4}\right)^{8.5} \tag{5}$$

Where C is a constant, ρ_0 the upstream flow density ($9.8 \times 10^{-5} \le \rho_0 \le 1.225\ kg/m^3$), V_0 the upstream flow velocity ($1828.8 \le V_0 \le 7924.8\ m/s$), and R_n the nose radius ($0.1016 \le R_n \le 0.9144\ m$).
However, the radiative heat flux of the gas can be neglected in comparison with the convective heat flux.

The radiation emitted from the wall to the flow is given by the Stefan-Boltzmann law :

$$\Phi_{rad,w} = \epsilon\sigma T_w^4 \tag{6}$$

Where ϵ is the material emissivity, σ the Stefan-Boltzmann constant ($J.s^{-1}.m^{-2}.K^{-4}$), and T_w the wall temperature (K).

The conductive heat flux is given by :

$$\Phi_{cond} = k \bigtriangledown T + \Phi_{diff} \tag{7}$$

where Φ_{diff} is the diffusive heat flux of species. $\Phi_{diff} = 0$ for a non catalytic wall and $\Phi_{diff} \neq 0$ for a catalytic wall.
In the first approach proposed here, the conductive heat flux at the stagnation point of the secondary sphere is supposed to be equal to zero. Indeed, because of the very thin wall thickness of the secondary hollow sphere, the temperature inside the sphere is supposed to reach the temperature outside almost instantaneously. Moreover, the wall is assumed to be non catalytic.

Fig. 14 to Fig. 17 display for different flight points the wall temperature (T_w) and total heat flux at the stagnation point of the secondary sphere ($\Phi_{tot} = \Phi_{conv} + \Phi_{rad,g} - \Phi_{rad,w}$), when the fragment interactions are (solid line) or not (dashed line) considered. The results are given from the axis ($r/R_s = 0$) to the shock ($r/R_s = 1$), for $\frac{d_1}{d_2} = 2$ and $\frac{x}{d_1} = 0.75$. The computations have been realized thanks to the present semi-analytical method for a real gas at thermochemical equilibrium. Wall temperature is obtained by assuming radiative equilibrium. Once melting point is reached, the temperature is set at this value and the convective and radiative heat fluxes are then computed. The melting point chosen for the computations is the titanium oxide one ($T_{melt} = 2130$ K). In fact, during the atmospheric re-entry, oxidation will appears almost instantaneously recovering the tank wall. Oxidation affects thermo-mechanical properties of the material and so could have an impact on the fragment survivability.

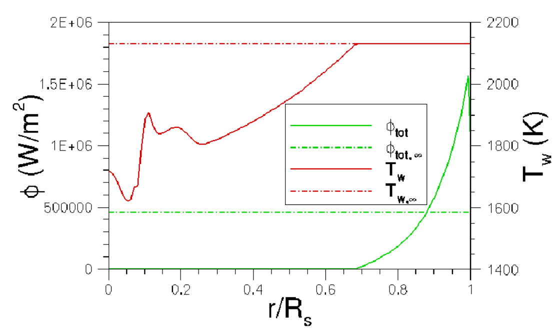

Figure 14. Comparison of the wall temperature and total heat flux on the secondary sphere at the stagnation point when fragment interactions are considered (solid line) or not (dashed line), for the following freestream conditions : $V_\infty = 7700\ m/s$, $H = 78\ km$.

Considering the evolution at the stagnation point of the secondary fragment wall temperature in the shock layer, two observations can be done from Fig. 14 to Fig. 17:
First, the protection conditions of the bow shock layer depends of the flight point conditions. Indeed, at the flight point $H = 50\ km$, $V_\infty = 7400\ m/s$ (Fig. 16) the melting temperature is reached whatever the fragment position along the r axis for $x/d_1 = 0.75$. So, the fragment

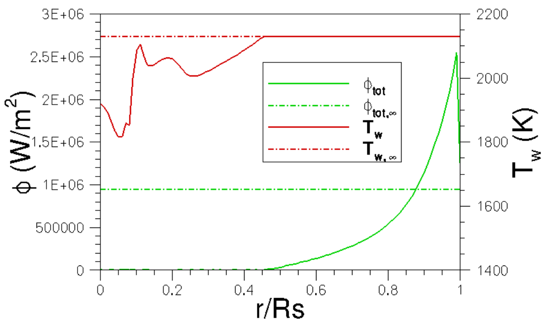

Figure 15. Comparison of the wall temperature and total heat flux on the secondary sphere at the stagnation point when fragment interactions are considered (solid line) or not (dashed line), for the following freestream conditions : $V_\infty = 7630\ m/s$, $H = 72\ km$.

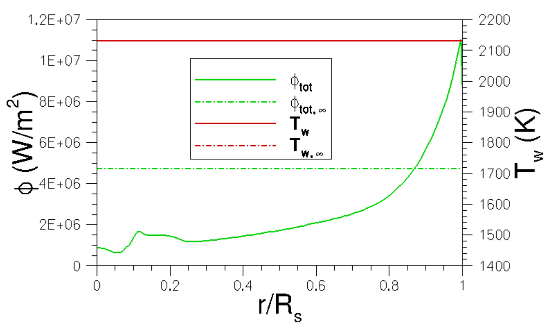

Figure 16. Comparison of the wall temperature and total heat flux on the secondary sphere at the stagnation point when fragment interactions are considered (solid line) or not (dashed line), for the following freestream conditions : $V_\infty = 7400\ m/s$, $H = 50\ km$.

is not protected by the primary one. Inversely, in Fig. 17 the melting temperature is never reached, meaning that the fragment remains completely protected at the flight point $H = 20\ km$ and $V_\infty = 2023\ m/s$.

Secondly, the protection conditions of the bow shock layer depends of the fragment position. In fact, as Fig. 14 and 15 shows, the melting temperature is not reached everywhere in the shock layer.

From present simulations, the protection conditions of the bow shock are flight dependent and also fragment position dependent.

REFERENCES

1. Ailor W. & al. (2006), A Strategy for Reducing Hazards from Reentry Debris, *AIAA paper*, 2006-6379.
2. Koppenwallner G., Fritsche B., Lips T., Klinkrad H. (2005), SCARAB-a multi-disciplinary code for destruction analysis of space-craft during re-entry, *Proceedings of the Fifth European Symposium on Aerothermodynamics for Space Vehicle*.

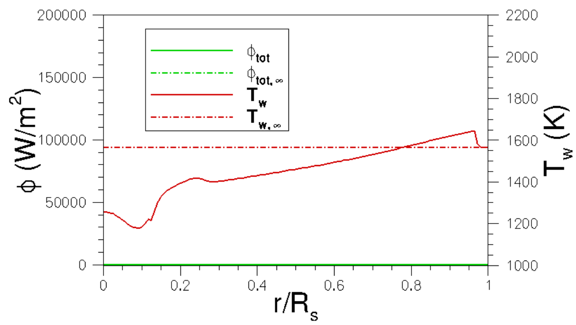

Figure 17. Comparison of the wall temperature and total heat flux on the secondary sphere at the stagnation point when fragment interactions are considered (solid line) or not (dashed line), for the following freestream conditions : $V_\infty = 2023\ m/s$, $H = 20\ km$.

3. Schultz P.H. and Sugita S. (1994), Penetrating and escaping the atmospheres of Venus and Earth, *Lunar and Planetary Science Conference XXV*, 1215-1216.
4. Laurence S.J., & al. (2007), Proximal bodies in hypersonic flow, *Journal of Fluid Mechanics*.
5. Sedov L.I. (1959), Similarity and Dimensional Methods in Mechanics.
6. Hayes W.D., Probstein R.F. (1959), Hypersonic flow theory, Academic Press.
7. Artemieva N.A., Shuvalov V.V. (1996), Interaction of shock waves during the passage of a disrupted meteoroid through the atmosphere, *Shock Waves*, 359-367.
8. Barri N. (2010), Basic aerodynamical properties of meteoroid fragments in the terrestrial atmosphere.
9. Passey Q.R. and Melosh H.J. (1980), Effects of Atmospheric Breakup on Crater Field Formation, *ICARUS*, 42.
10. Artemieva N.A., Shuvalov V.V. (2001), Motion of a fragmented meteoroid through the planetary atmosphere, *Journal of geophysical research*, 106, 3297-3309.
11. Vashchenkov P., Kashkovsky A., and Ivanov M. (2003), Aerodynamics of fragment in Spacecraft Wake, *Rarefied Gas Dynamics : 23rd International Symposium*.
12. Billig F.S. (1967), Shock-Wave Shape around Spherical- and Cylindrical-Nosed Bodies, *Journal of Spacecraft and Rockets*, 4 (6).
13. ONERA (2009), Manuel utilisateur de la chaine CEDRE, CEDRE 3.2.2.
14. R.L.Kelley, W.C.Rochelle, Atmospheric Reentry of a Hydrazine Tank.
15. P.Sagnier, J-L.Verant (1998), Flow Characterization in the ONERA F4 high enthalpy wind tunnel, *AIAA Journal*, Vol.36, No. 4, 522-531.
16. J.J.Martin (1966), Tmospheric Re-entry, An Introduction to its Science and Engineering, *Prentice-Hall, Englewood Cliffs*.